IEEE Open Journal of
Circuits and Systems

Received 4 April 2021; revised 12 July 2021; accepted 28 July 2021. Date of current version 13 September 2021.

Digital Object Identifier 10.1109/OJCAS.2021.3105005

Towards the Co-Simulation of Charge Qubits: A Methodology Grounding on an Equivalent Circuit Representation

ELENA BLOKHINA [1,2] (Senior Member, IEEE), ANDRII SOKOLOV [1,2], PANAGIOTIS GIOUNANLIS [1], XUTONG WU [1,2], IMRAN BASHIR [3] (Member, IEEE), DIRK LEIPOLD [3] (Senior Member, IEEE), ROBERT BOGDAN STASZEWSKI [1,2] (Fellow, IEEE), ANGELO BRAMBILLA [4] (Member, IEEE), AND FEDERICO BIZZARRI [4,5] (Senior Member, IEEE)

1 Equal1 Labs Ltd., Dublin 4, Ireland
2 School of Electrical and Electronic Engineering, University College Dublin, Dublin 4, Ireland
3 Equal1 Labs Inc., Fremont, CA 94536, USA
4 DEIB, Politecnico di Milano, 20133 Milano, Italy
5 Advanced Research Center on Electronic Systems for Information and Communication Technologies E. De Castro, University of Bologna, 41026 Bologna, Italy
This article was recommended by Associate Editor D. Galayko.

CORRESPONDING AUTHOR: P. GIOUNANLIS (e-mail: panagiotis.giounanlis@equal1.com)

This work was supported in part by Enterprise Ireland through Disruptive Technologies Innovation Fund under Grant DT 2019 0090C.

ABSTRACT This paper presents a methodology to describe quantum mechanical states of charge qubits, realized as coupled quantum dots occupied by single electrons, using equivalent electrical circuits. We explain how to construct all equations starting from low-level simulations of wave functions and interpret the relationship between the parameters appearing in the resulting model and the parameters of the physical system. An efficient methodology to obtain 2D wave functions is presented. Results obtained in this study using a circuit simulator correspond to quantum dot arrays fabricated in a CMOS technology and recently published in the literature. The generalization of quantum mechanical equations, their conversion to equivalent circuits, and numerical examples are discussed.

INDEX TERMS Quantum dot arrays, quantum electronics, Hamiltonian matrix, charge qubit simulations, equivalent circuits, circuit simulation.

I. INTRODUCTION

COMPUTING systems based on quantum mechanical properties of superposition, interference and entanglement are known as quantum computers (QC) [1]. They operate on quantum bits (qubits), analogues of the elementary unit of information used in the theory of quantum computation. The concept of the quantum computer originated from the idea that in order to efficiently simulate a quantum system, another quantum system should be used rather than a classical computer [2]. For some quantum algorithms, such as the Shor's integer-factorization algorithm [3], it has been proven that it can outperform its classical counterpart. At the moment, many algorithms and applications for quantum computing have been proposed [4], some tested in available frameworks such as IBM Qiskit, and some tried in existing quantum computers. Operational quantum computers and processors have been actively reported in recent years in the literature, while IBM offers access to their quantum computers [5].

In addition to the superconducting transmon qubit technology dominating at the present [6]–[8], many other qubit technologies are available. Photonic systems [9], [10], trapped ions [11] and semiconductor quantum dots [12] are also recognized as an option to implement quantum processors. The current generation of quantum computers is often called Noisy Intermediate Scale Quantum (NISQ) to highlight that the count and quality of operational qubits are not enough to fully leverage "quantum supremacy" [4], [8], [13], but enough to test some of the algorithms and applications.

We focus on the semiconductor qubit technology for the reasons we outline in this paragraph. In this technology, a qubit is implemented employing an electron's spin, charge or both (a so-called "hybrid qubit") using the concept of a quantum dot (QD). The role of a QD is to create a spatial confinement for electrons or holes using an electric field arising either from material interfaces or by applying a confining electric potential. Semiconductor QDs have been known for about two decades [12], [14]–[20]. Key reason that makes semiconductor QDs very attractive in the context of circuit design is that they can be now implemented using Complementary Metal-Oxide-Semiconductor (CMOS) or foundry fabricated technologies [21]–[24] since the quality and reliability of commercial processes have dramatically increased [25]. Improving the material purity with finer lithographic processes, increasing the switching speed of transistors, and decreasing the size of transistors facilitate the implementation of qubits together with the integration of control electronics on the same chip. It has been recently postulated that this may open an avenue to finally achieve a large number of qubits within a single quantum processor [26]–[32]. Finally, one may note that while the superconducting qubits require ultra low temperatures (10 mK), some quantum dots have been shown to operate at higher temperatures (1 K) [33]. A reader interested in silicon quantum electronics will find many relevant results accumulated in the review paper [34].

The aim of this paper is to outline a methodology to convert the Hamiltonian dynamics of a quantum mechanical system into an equivalent circuit representation. We note that this representation will not be able to reduce the computational resources and time required to simulate qubits (as it does not solve the issue of the exponentially increasing state space). However, this allows one to co-simulate the quantum mechanical equation with the electronic circuitry driving and controlling qubits in a unified environment that may be useful for system verification and convenient for integrated circuit (IC) designers.

In this paper, we have chosen an example of a quantum dot array recently implemented in a CMOS technology together with their interface electronics [22], [35]. We propose and discuss in detail a modeling methodology particularly focused on the side of the problem that may be appealing to readers with background in circuit design. Indeed, in light of the rise of semiconductor and CMOS quantum technologies, recasting quantum mechanical equations into the form of electrical networks (e.g., one of the fundamental examples is presented in [36]) can be useful for a number of reasons. Firstly, it allows one to co-simulate the evolution of wave functions together with control electronics and leverage simulation packages for circuits, which are currently at a very progressed stage. Secondly, this representation may be perceived as more conventional to engineers and circuit designers.

The paper is organized as follows. In Section II, we provide the description of the system and mathematical formalism. Section III outlines 2-dimensional simulations and a method to obtain a Hamiltonian matrix. The generalization of the description is presented in Section IV. In Section V, we propose an equivalent circuit approach, and Section VI presents numerical examples.

II. STATEMENT OF THE PROBLEM

A. DESCRIPTION OF THE STRUCTURE UNDER STUDY

We will consider an example of a semiconductor quantum dot array inspired by the structures published recently in the literature [21], [22], [31], [35], [37], [38]. In particular, the dimensions, material composition and material properties used in this paper for modeling and simulations correspond to the devices presented in [22] and fabricated in a 22-nm CMOS node of fully depleted silicon-on-insulator (FDSOI) from GlobalFoundries. The description of the structure, including some technology elements, is presented in Fig. 1. Information on the composition of layers and materials can be found, for instance, in [39], [40].

This structure can be seen as a string of reduced transistors. It contains multiple gates along the depleted silicon channel and highly doped source/drain terminals at the edges of the structure. The electrical control of confinement, charge injection and charge detection are implemented using 'classical' integrated circuitry. The electrical contacts that interface the control circuitry are labeled in this schematic as *imposers* and *floating nodes*. Electrons injected into the depleted silicon channel from the edges of the structure follow the electrical control from the imposers. This means that the DC voltage applied at the imposers combined with the voltage arising from the semiconductor material interfaces create quantum dots in the silicon channel. Once injected into the channel, the electron behavior is described by the Schrödinger equation through a wave function resulting from the potential energy developed in the channel. The injection and detection of electron(s) in the silicon channel is implemented using a technique known as *floating source/drain* concept, which is quite commonly used in charged-coupled devices [41]. With some modifications (in the configuration of a *floating gate*), a similar technique, known as a *single-electron detection*, has been utilized with quantum dots and qubits [42]. The floating nodes are not connected directly to any voltage or current sources. Other measurement techniques, such as RF reflectrometry, can also be used [21], [43].

The potential energy seen by the electron(s) in the channel can be calculated if the voltages applied at the imposers are known. In the simplest case of one electron moving in an electric field whose scalar electric potential is $V(x, y, z)$, the potential energy is $U = -eV$, where e is the magnitude of electron charge, and x, y, z are the three orthogonal spatial coordinates. The case of many electrons is more complicated and will require to calculate the interactions between them. The potential energy is plugged into the Schrödinger equation and relates the "classical" electrical domain with the "quantum" domain. The Schrödinger equation is written in

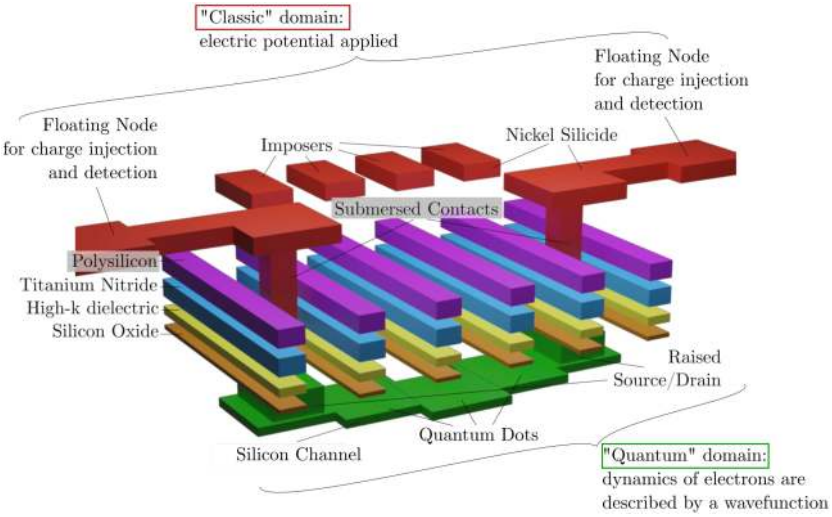

FIGURE 1. Schematic view of the system under study showing some technology details. The TEM photograph of the structure can be seen in Fig. 2(c) with further details found in [22]. The electrical control of confinement, charge injection, and charge detection are implemented using 'classical' integrated circuitry [35]. The electrical contacts that interface the control circuitry are labeled in this schematic as *imposers* and *floating nodes*. Electrons, injected in the depleted silicon channel from the edges of the structure, follow electrical control from the imposers. The electron behavior is described by the Schrödinger equation through a wave function resulting from the potential energy developed in the channel.

terms of a complex-valued wave function $\Psi(x, y, z, t)$ whose magnitude squared gives the probability to locate an electron in a given region of space.

To be more specific, we will consider two particular cases, shown schematically in Fig. 1. The first case is quite simple since it looks into the dynamics (equilibrium oscillations) of one electron confined in three dots (see Fig. 1(a)). Despite its simplicity, this example extends beyond the standard two-level (two-dot) system, and can be easily expanded into the case of one electron confined in an arbitrary number of dots. The second case is more interesting as it considers two interacting quantum dot arrays, each consisting of three dots (see Fig. 1(b)). With this example, we demonstrate how to model the Coulomb interaction between electrons.

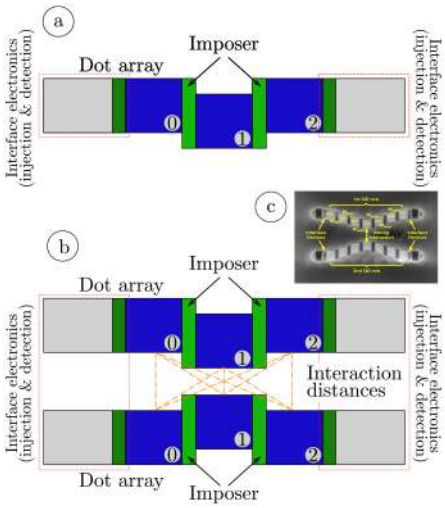

FIGURE 2. Two particular examples considered in this study: (a) a quantum dot array consisting of three dots, (b) two interacting quantum dot arrays, α and β, each consisting of three dots, (c) a photograph of dot arrays (from [22]). Each dot array edge is connected to interface circuitry performing charge injection and detection (schematically denoted by a gray rectangle and highlighted by red dashed lines). Structures denoted as imposers are MOS transistor gates controlling the local electric field.

B. MATHEMATICAL FORMALISM

This short tutorial section summarizes the basic ideas from Quantum Mechanics used in the paper with the purpose of reminding the reader about these concepts, their role and connections to observable quantities in this system. For an introduction to this field, we can suggest one of many textbooks on the topic, such as [44]–[46].

The fundamental equation of quantum wave mechanics is the time-dependent Schrödinger equation written, for instance, in a 3-dimensional (3D) Cartesian space for one particle:

$$i\hbar\frac{\partial\Psi(x,y,z,t)}{\partial t} = \left[-\frac{\hbar^2}{2m_e^*}\nabla^2 + U(x,y,z,t)\right]\Psi(x,y,z,t), \tag{1}$$

where $\hbar$ is the reduced Planck's constant, i is the imaginary unit, m_e^* is the effective mass of the particle (electron in our case), and $U(x, y, z, t)$ is the potential energy function. The complex-valued wave function $\Psi(x, y, z, t)$ describes the dynamics of the particle in space and time. The potential energy of the electron, as mentioned earlier, is obtained from the electric fields (or scalar electric potentials) acting on the particle. The Schrödinger equation can formally be written also for an M-particle case assuming that the wave function becomes a function of the respective coordinates of the particles $\Psi(x_1, y_1, z_1, \ldots x_M, y_M, z_M, t)$. The wave function and its derivatives are continuous, and the wave function itself

is normalized:

$$\int_{\infty} |\Psi(x, y, z, t)|^2 \, \mathrm{d}v = 1 \,, \tag{2}$$

where $\mathrm{d}v$ denotes the infinitesimal volume element (in Cartesian coordinates $\mathrm{d}v = \mathrm{d}x\,\mathrm{d}y\,\mathrm{d}z$). The wave function itself has no interpretation, but its magnitude squared can be interpreted as the probability density function, giving information about the location of the particle:

$$\Pr(x, y, z, t) = |\Psi(x, y, z, t)|^2. \tag{3}$$

The straightforward solution of this equation is very problematic for many reasons. Firstly, solving it in three dimensions and time is extremely resource consuming. Even though many efficient numerical schemes exist [47], solving this equation for a given configuration of parameters provides little insight into the physics of a given system. In addition to that, even though the formal extension to the many-particle case can be made, additional information is required to handle symmetrization and antisymmetrical in the bosonic and fermionic cases.

The first simplification is made when the time-independent Schrödinger equation is introduced by separating the variables in $\Psi(x, y, z, t) = \sum_n A_n \cdot \exp(-iE_n t/\hbar)\psi_n(x, y, z)$:

$$\left[-\frac{\hbar^2}{2m_e^*}\nabla^2 + U(x, y, z)\right]\psi_n(x, y, z) = E_n\psi_n(x, y, z)\,, \tag{4}$$

where E_n are the eigenenergies of the system and $\psi_n(x, y, z)$ are their corresponding eigenfunctions. This variable separation is valid when the potential function of the system is constant (and is also held in some particular cases of time-dependent energy functions). The time-independent Schrödinger equation allows one to solve many practical examples, analytically or numerically, and obtain the set of space-dependent functions $\psi_n(x, y, z)$ and energies E_n of the system. The eigenfunctions ψ_n are normalized and orthogonal:

$$\int_{\infty} \psi_m^* \psi_n \, dv = \langle\psi_m|\psi_n\rangle = \delta_{mn}\,, \tag{5}$$

where δ_{nm} is the Kronecker delta symbol, and the symbol $*$ means complex conjugation. The expression above makes use of the Dirac notation that draws analogies between quantum mechanics and the algebra of complex vector spaces. Using this notation, equation (4) can be written in the form $\hat{H}|\psi_n\rangle = E_n|\psi_n\rangle$ where the operator $\hat{H} = [-\frac{\hbar^2}{2m_e^*}\nabla^2 + U(x, y, z, t)]$ is the total energy (Hamiltonian) operator giving the energy of the system. Thus, E_n are the eigenvalues and ψ_n are eigenfunctions of the operator $\hat{H}$.

Assuming that a set of orthonormal functions ϕ_n is given, by presenting the full wave function in the form $\Psi(x, y, z, t) = \sum c_n(t)\phi_n(x, y, z)$, and plugging it into equation (1), we obtain:

$$i\hbar\frac{\mathrm{d}c_m}{\mathrm{d}t} = \sum_n H_{mn}c_n, \tag{6}$$

where

$$H_{mn} = \int \phi_m^*(x)\hat{H}\phi_n(x)\mathrm{d}v = \langle\phi_m|\hat{H}|\phi_n\rangle. \tag{7}$$

By doing so, the time-independent Schrödinger equation is written as a set of ordinary differential equations (ODE) in terms of the coefficients c_n. We note that if the set of functions ϕ_n represents the eigenfunctions of the energy operator $\phi_n \equiv \psi_n$, the Hamiltonian matrix $\hat{H}$ in expression (7) will be diagonal. For any other orthonormal set ϕ_n, the Hamiltonian matrix $\hat{H}$ contains non-diagonal terms. As follows from expression (7), matrix $\hat{H}$ is Hermitian (or self-adjoin) implying $\hat{H} = \hat{H}^\dagger$.

Hence, solving a problem in the context of time-independent wave mechanics requires one to obtain the functions ϕ_n that provide the information about the probability density of particle(s) in a given potential energy, calculating the matrix elements H_{mn} (7) and solving the set of ODEs (6). In the next section, we show how to carry out the calculations by the two examples we described earlier in this section.

III. NUMERICAL SIMULATIONS OF THE SPATIAL WAVE FUNCTIONS OF ONE ELECTRON IN A QUANTUM DOT ARRAY

This section shows how to connect the potential energy (expressed through the circuit voltage that drives qubits) and the system dimensions with the eigenenergies and wavefunctions in the Schrödinger equation. This methodology corresponds to the realistic devices and technology [22], [35] and results in the parameter values used throughout this work.

Firstly, we start with the one-electron case. We consider a 2D QD array consisting of two and three dots. The schematic of the top-view 2D geometry is shown in Fig. 3. To calculate the wave functions, we will need to specify the potential energy $U(x, y)$ as a function of the spatial coordinates x and y. To obtain $U(x, y)$, we need to calculate the electric potential in the silicon channel in response to the voltages applied at the imposers and developed in the floating nodes. As briefly outlined in [37], a typical depth of the potential (quantum) well in the channel is about 5 meV. For the calculations in this paper, we assume that the bottom of the well is at 0 meV, the potential energy barrier separating two neighboring dots is $U_{\mathrm{bar}} = 10$ meV, and these confining potentials are 'embedded' into another potential of $U_{\mathrm{board}} = 1$ eV that reflects the electric fields due to the material interface (silicon channel vs. insulating materials).

To find the eigen wave functions ψ_j and eigenenergies E_j we solve the time-independent Schrödinger equation of an electron in a 2D electrostatic potential:

$$\left\{-\frac{\hbar^2}{2m_e^*}\left[\frac{\partial^2}{\partial x^2} + \frac{\partial^2}{\partial y^2}\right] - eV(x, y)\right\}\psi_j(x, y) = E_j\psi_j(x, y),$$

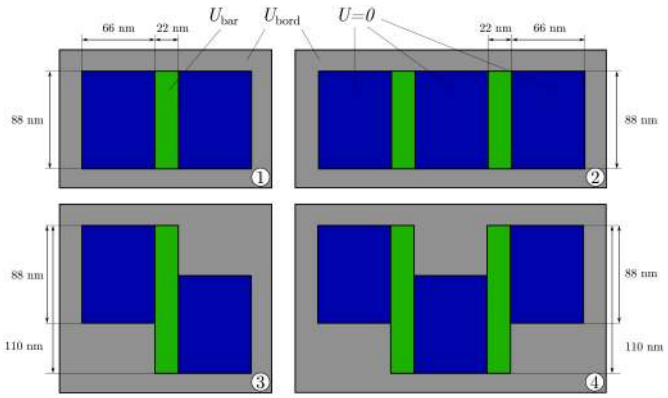

FIGURE 3. Geometry of the one-electron case study. The main case we focus on is geometry 4 with three dots having a step shift between the middle dot and the edge dots. The other three cases can also be easily calculated using the presented methodology. The bottoms of the confining potential wells are set to zero potential energy. The potential energy of the barriers separating the wells is set as $U_{bar} = 20$ meV (denoted by the green color). The structures are embedded into a global potential well $U_{bord} = 1$ eV (denoted by the grey color).

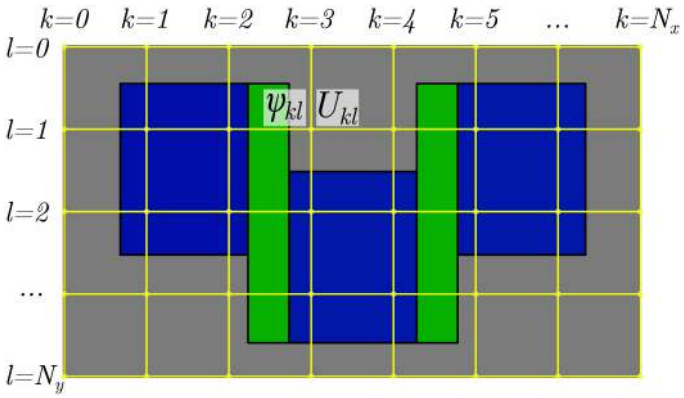

FIGURE 4. Illustration of a finite difference method used in this study to obtain an estimate of the eigenenergies and eigenfunctions of the time-dependent Schrödinger equation. For the QD arrays with the dimensions as shown in Fig. 3, a square mesh with a cell of 2 nm is applied. As a result of the calculations, a set of matrices containing discretised functions ψ^j_{kl} is obtained.

(8)

where the constants appearing in the above equations are the same as in equation (1), and $V(x, y)$ is the scalar electric potential (voltage) in the silicon channel. The potential energy $U(x, y) = -eV(x, y)$ is indicated in Fig. 3. In this study, we look into the formation of the lateral confinement wells in the structure.

We can reduce the problem of finding the eigensystem (energies and functions) of the Hamiltonian energy operator (8) to finding the eigenvectors and eigenvalues of a sparse matrix, which is a very common task in physics and engineering. In our case, we use the 'scipy' package of Python. To do this, we apply a square mesh to the wave function $\psi_j(x, y)$ and use a standard finite-difference method with zero boundary conditions (these conditions are imposed since we assume that the injected electron is localized somewhere in the QD array). The numerical method returns a set of energies E_j and a set of corresponding wave functions $\psi_j(x_{kl}, y_{kl})$, defined at the discrete nodes of the mesh, as shown in Fig. 4. They provide an estimate of the eigenenergies and eigenfunctions of the original problem.

Note that there are some inherent features of the finite difference method when applied to our problem. The method works with matrices of a very high rank $N_x^2 \times N_y^2$, where N_x and N_y are the number of nodes in the mesh in the x- and y-dimensions. However, while the matrix may be extremely large, it almost fully consists of zeros. Compressed formats to store the matrix in the PC's RAM can be used, and there are specific stochastic methods developed for sparse matrices to obtain their eigenvalues. For this reason, this computational technique can be made very efficient in 2D cases. We also note that the obtained wave functions are normalized $\langle\psi_i|\psi_j\rangle = \delta_{ij}$.

To understand if our method is self-consistent, we compare the eigenenergies obtained from this method (E_j) with the energy expected from a given function (ψ_j) by applying the Hamiltonian operator to it:

$$\varepsilon = \frac{\left|\langle\psi_j|\hat{H}|\psi_j\rangle - E_j\right|}{E_j}. \tag{9}$$

We calculate the term $\hat{H}\psi_j$ in the above equation by using the discrete representation of the second derivative:

$$\hat{H}\psi(x, y) \simeq -\frac{\hbar^2}{2m_e^*}\left[\frac{\psi_{i,j+1} - 2\psi_{i,j} + \psi_{i,j-1}}{\Delta x^2} + \frac{\psi_{i+1,j} - 2\psi_{i,j} + \psi_{i-1,j}}{\Delta y^2}\right] + U_{i,j}\psi_{i,j}. \tag{10}$$

The error obtained from expression (9) in our simulations is less than 1% for the mesh reported in Fig. 4.

It is very important to highlight that by solving equation (8), we obtain eigenfunctions in the *energy representation* (since each function ψ_j appears together with the corresponding energy E_j), and these eigenfunctions diagonalize the matrix (7). However, quantum mechanics allows one to straightforwardly convert between different representations by applying an appropriate unitary transform. Why should we apply this transform? Eigenfunctions in the energy representation may have spatial distributions that do not correspond to localised electron states.

This example is demonstrated in Fig. 5 where the left panel of wavefunction subfigures presents the probability density $\Pr(x, y)$ corresponding to the first three eigenstates: state $|0\rangle$ expressed by the function $|\psi_0(x, y)|^2$ with E_0 (the very first state with the lowest eigenenergy E_0 is usually called the ground state), state $|1\rangle$ expressed by $|\psi_1(x, y)|^2$ with E_1, and state $|2\rangle$ expressed by $|\psi_2(x, y)|^2$ with E_2. One can see that while the state given by the function $\psi_0(x, y)$ corresponds to the localization of the injected electron in the middle dot, the other two states $\psi_1(x, y)$ and $\psi_2(x, y)$ are 'delocalised'.

This delocalization actually plays a very important role. Depending on the potential energy, its symmetry and the

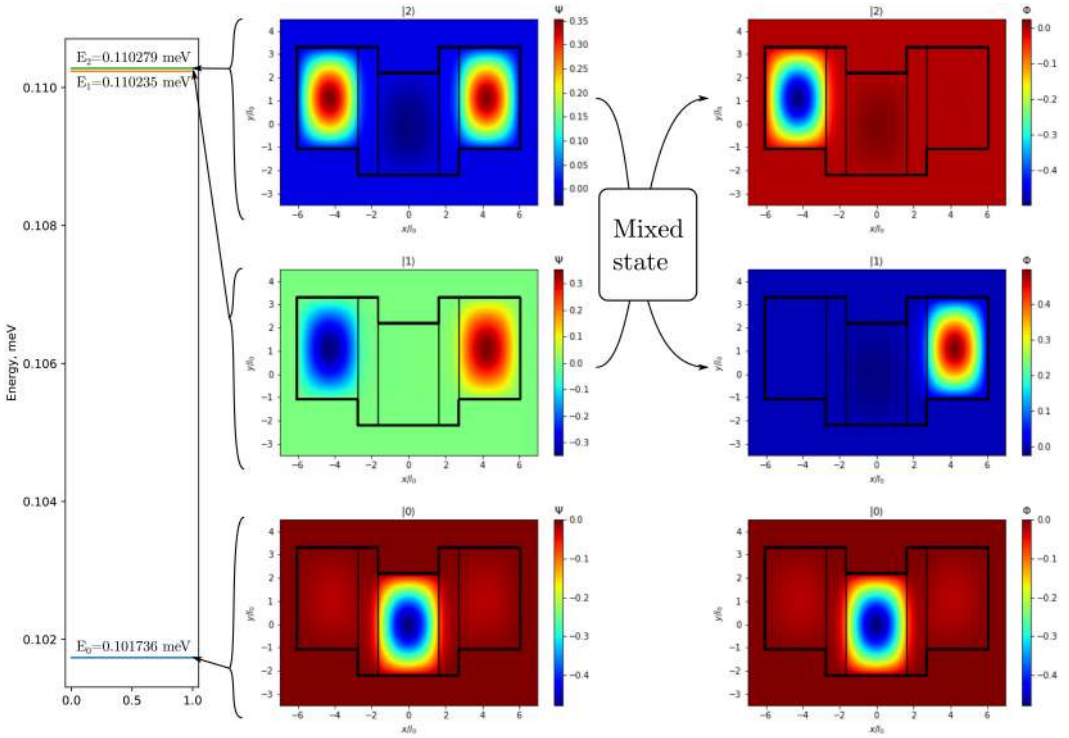

FIGURE 5. Left panel of the wavefunctions: the probability densities of the first three eigenstates: $|\psi_0(x, y)|^2$ with E_0, $|\psi_1(x, y)|^2$ with E_1, and $|\psi_2(x, y)|^2$ with E_2, showing that the eigenfunctions ψ_1 and ψ_2 are delocalised (or hybridized) allowing a wavefunction overlap. This representation is called the energy representation. Right panel of the wavefunctions: a linear transform is applied to switch to the position representation where the probability densities correspond to localised states. The bar on the left of the figure shows energy spectrum of these three eigen wavefunctions. The wavefuncitons are plotted against the normalized coordinate x_0/L where $L = 20$ nm is the technology feature size.

height of the barriers separating the quantum dots, the eigen wavefunctions can represent solutions localized in the first, second and third dots, respectively. Decreasing the height of the potential barrier results in a hybridization of some wavefunctions and split of the energy levels. The case of the eigen wavefunctions becoming 'delocalised' is presented in Fig. 5. As we will see later, this delocalization will allow transitions between the states and results in the equilibrium dynamics presented in the sections. Note how the eigenenergies for the excited states ($|1\rangle$ and $|2\rangle$) are very close (but not exactly the same).

However, if we want to use this result to model the behavior of the classical charge detection circuit, we would rather know the amount of charge in each of the dots than the system's energy. For this reason, it may be convenient for us to switch to *position representation* by applying a linear transform. This transform leaves the ground state unaffected but changes the other two states, as shown again in Fig. 5 in the right panel of subfigures.

Mathematically, we can express this transformation as follows:

$$\begin{cases} \phi_0(x, y) = \psi_0(x, y), \\ \phi_1(x, y) = \frac{1}{\sqrt{2}}(\psi_1(x, y) + \psi_2(x, y)), \\ \phi_2(x, y) = \frac{1}{\sqrt{2}}(\psi_1(x, y) - \psi_2(x, y)). \end{cases} \tag{11}$$

The functions $\phi_j(x, y)$ are orthonormal but are not the eigenfunction of the Hamiltonian operator anymore and will not diagonalize the matrix (7). Expression (7) still applies in this case:

$$\begin{aligned} H_{ij} &= \iint \mathrm{d}x\mathrm{d}y\phi_i(x, y) \cdot \left[\hat{H}\phi_j(x, y)\right] \\ &\simeq \mathrm{d}x\mathrm{d}y \sum_{i=0}^{N_x} \sum_{j=0}^{N_y} \phi_{kl}^{(i)} \left[\hat{H}\phi_{kl}^{(j)}\right]. \end{aligned} \tag{12}$$

Hence, if we limit ourselves to the first three states, the dynamics of the system will be described by equation (6) and we can write down three equations for the probability amplitudes (c_0, c_1, c_2) of states (ϕ_0, ϕ_1, ϕ_2). The Hamiltonian matrix is a 3×3 matrix with the elements H_{ij}, $i = 1, 2, 3$ and $j = 1, 2, 3$ calculated numerically using expression (12).

Finally, we expand this formalism to our second case of two interacting electrons shown in Fig. 2(b). The combined wave function describing the two electrons $\phi = \phi^\alpha \otimes \phi^\beta$ is obtained by applying the tensor product to the function ϕ^α of the electron in the upper QD array (line α) and to the function ϕ^β of the electron in the lower QD array (line β). The Hamiltonian matrix will require adding additional terms describing the Coulomb interaction (more details will be given when we discuss formula (17)):

$$H_{ij}^{\mathrm{int}} = \langle \phi_i\phi_j \big| U_{\mathrm{int}}\big(x_i, y_i, x_j, y_j\big) \big| \phi_i\phi_j \rangle, \tag{13}$$

where the potential energy of the interaction between two electrons can be found from the Coulomb Law:

$$U_{\text{int}}(x_i, y_i, x_j, y_j) = \frac{1}{4\pi\varepsilon_r\varepsilon_0}\frac{e^2}{\sqrt{(x_i - x_j)^2 + (y_i - y_j)^2}}, \quad (14)$$

where ε_0 is the permittivity of the free space and ε_r is the relative permittivity of the medium where the interaction takes place (in our case, the electrons are placed in silicon). Note that (13) requires resource-intensive calculations since it contains a 4-D integral. For this reason, a custom low-level high-performance C-code is developed to calculate this term.

Finally, we note that the following workflow has been employed to obtain useful results. We perform electromagnetic calculations using a finite-element method (FEM) solver to calculate the potential energy $U = -eV$. This energy is used in eq. (8) to calculate the wave-functions and Hamiltonian matrices that correspond to this potential energy. The relationship between the Hamiltonian matrix elements and driving voltages can be approximated by some nonlinear function and later used in the circuit solver described in this paper to avoid unnecessary invoking of FEM solvers.

IV. GENERALIZATION OF THE APPROACH USING THE SECOND QUANTIZATION FORMALISM

In this section, we aim to show a generalization of the approach to generate the set of ODEs, vectors and Hamiltonian matrices using the formalism of the *second quantization* method. This is a method that is straightforward to read and expand to an arbitrary number of electrons and quantum dots. This method, as an illustration, will be applied to the two case studies presented in Fig. 2. Note that the method is particularly suitable for multi-electron systems. Using this method, the state of the system is represented by a vector containing *occupation numbers*:

$$|n\rangle = |n_1\, n_2\, \ldots, m_1\, m_2 \ldots\rangle, \quad (15)$$

where the occupation number n_j represents the occupation of the j^{th} 'state' associated with line α and the occupation number m_j represents the occupation of the j^{th} state associated with line β. In the fermionic case, which applies to electrons, there is an additional restriction that two fermions cannot occupy the same state. Hence, each occupation number can be either zero or one: $n_j = \{0, 1\}$ and $m_j = \{0, 1\}$. Each occupation number n_j is associated with the creation and annihilation operators $\hat{c}_j^\dagger$ and $\hat{c}_j$ so that $\hat{n}_j = \hat{c}_j^\dagger \hat{c}_j$ is the occupation number operator for a state labeled with index j.

Furthermore, the excitation operator $\hat{c}_i^\dagger \hat{c}_j$ is introduced. This operator removes an electron from the j^{th} state and places it in the i^{th} state. Its Hermitian conjugate is the operator $\hat{c}_j^\dagger \hat{c}_i$ that, vice versa, removes an electron from the i^{th} state and places it in the j^{th} state. If we want to consider more than one electron, we can use the notations $\hat{c}_{\alpha,j}^\dagger$, $\hat{c}_{\alpha,j}$ and $\hat{c}_{\beta,j}^\dagger$, $\hat{c}_{\beta,j}$ for the creation and annihilation operators acting in lines α and β, respectively. Hence, in the most general case, these operators will be denoted as $\hat{c}_{i,j}^\dagger$ and $\hat{c}_{i,j}$, where $i = \alpha, \beta$ and $j = \{1, \ldots, N\}$ with N representing the total number of states for an electron in each line. This labeling approach can be easily extended to an arbitrary number of lines (electrons) with an arbitrary number of states.

If we want to present the first case study (one electron oscillating in three dots, Fig. 2(a)) using second quantization, we can use, for convenience, the position representation, agreeing that the states $|0\rangle$, $|1\rangle$ and $|2\rangle$ will correspond to the occupations of the dots in the pre-defined order. For example, we can agree that $|0\rangle$ corresponds to the occupancy of the middle dot, and $|1\rangle$ and $|2\rangle$ correspond to the occupancy of the left and right edge dots. (While this may seem odd, the order of these labels reflect the energy levels rather than direct labeling of the dots from right to left.) The three-dot system is described by the following Hamiltonian matrix:

$$\hat{H} = \begin{array}{c} \\ \langle 0| \\ \langle 1| \\ \langle 2| \end{array} \begin{array}{c} \begin{array}{ccc} |0\rangle & |1\rangle & |2\rangle \end{array} \\ \begin{bmatrix} E_{p0} & t_{h,01} & t_{h,02} \\ t_{h,10} & E_{p1} & t_{h,12} \\ t_{h,02} & t_{h,21} & E_{p2} \end{bmatrix} \end{array}, \quad (16)$$

where the tunneling (or hopping) terms $t_{h,ij}(t) = \tau_{h,ij}(t) - i\,\alpha_{h,ij}(t)$ $(i, j = 0, 1, 2$ with $i \neq j)$ describe the transition of the electron between the i^{th} and j^{th} dots and E_{pj} $(j = 0, 1, 2)$ describe the energy the electron possesses in the j^{th} dot. The tunneling terms *can be* complex valued.

The tunneling coefficients are complex valued in the most general case since they are obtained by integrating two generally complex-valued wavefunctions with the Hamiltonian operator. The complex value reflects either the presence of a phase shift between the wavefunctions corresponding to the respective states (which could happen, for example, due to initial conditions) and/or the appearance of an additional phase shift due to specific physical interactions in the system. (A phase shift is usually induced due to the Aharonov-Bohm effect that can be electrical or magnetic.) The presence of the imaginary part of a Hamiltonian matrix due to some phase difference between the eigenfunctions is not necessarily physically meaningful. For example, it can contribute to the phase-factor of the entire matrix, known as the global phase, that is not observable. For simplicity, in the paper we have imposed specific conditions so that the eigenfunction are real valued, and the resulting Hamiltonian is real valued, too.

We note that the states $|j\rangle$ in equation (16), with $j = 0, 1, 2$, need not be necessarily written in the position representation, implying that an electron is physically occupying a given dot. This is a convenient representation, but not the only one possible. One can think of an electron physically occupying a quantum dot (position representation) or occupying an energy level (energy representation). Since the wave function vector and the creation and annihilation operators are rather abstract concepts, switching between the two representations only involves the unitary transform as described by formula (11) and this can be very easily done for single electron examples.

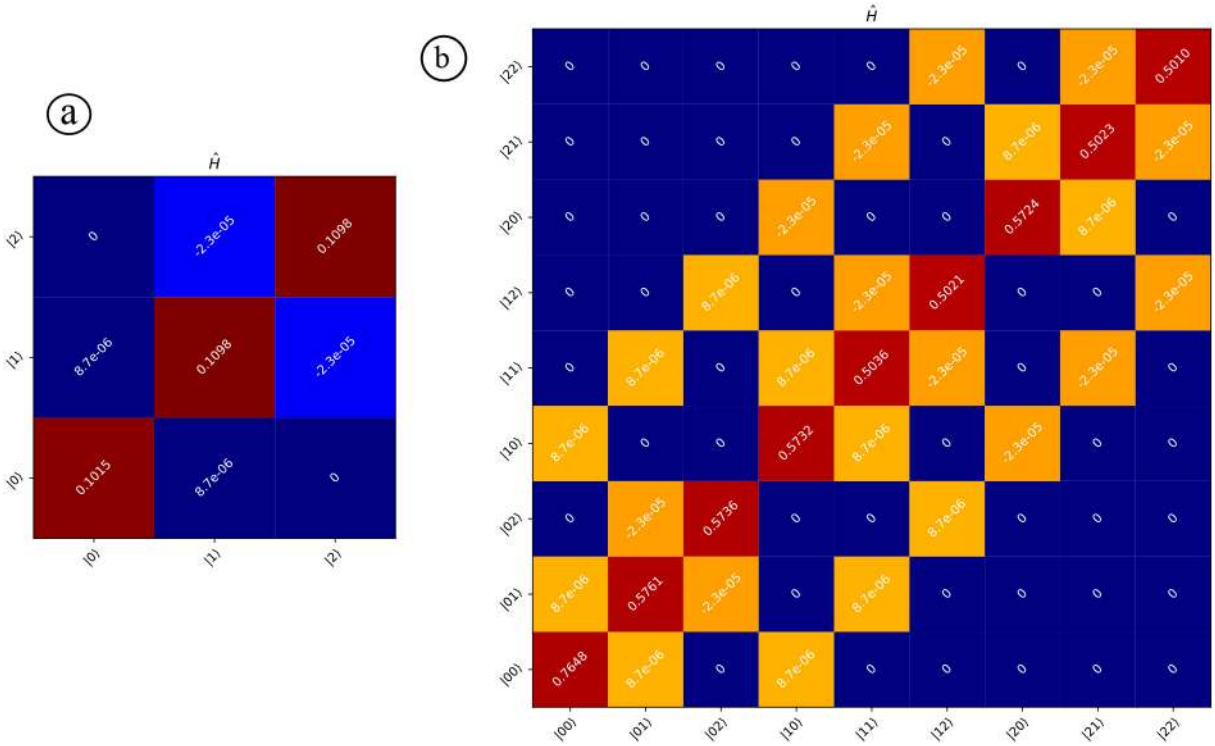

FIGURE 6. (a) Hamiltonian matrix of the three-dot array case study from Fig. 2(a). It is a 3×3 matrix describing transitions between state $|0\rangle$ (occupancy of the middle dot), state $|1\rangle$ (occupancy of the left dot) and state $|2\rangle$ (occupancy of the right dot). (b) Hamiltonian matrix of the dual three-dot array case study from Fig. 2(b). It is a 9×9 matrix describing transitions between the state of the upper and lower lines $|n\rangle \otimes |m\rangle$. Here $|n\rangle = |0\rangle, |1\rangle$ or $|2\rangle$ describe the occupation of the middle, left and right dots in the upper line and $|m\rangle$ describes that of the bottom line. The energies in these Hamiltonian matrices are given in meV.

With regard to the second case study (two interacting electrons in Fig. 2(b)), we create the Hamiltonian matrix as follows:

$$\hat{H} = \hat{H}^{(\alpha)} \otimes \hat{I} + \hat{I} \otimes \hat{H}^{(\beta)} + \hat{H}^{\text{int}}, \tag{17}$$

where $\hat{H}^{(\alpha)}$ and $\hat{H}^{(\beta)}$ are the Hamiltonian matrices each describing its respective lines. The component $\hat{H}^{\text{int}}$ represents the Coulomb interaction between the two electrons, and $\hat{I}$ is the identity matrix. The tunneling terms are still denoted as $t_{h,ij}(t)$ where $h = \alpha, \beta$ and $i, j = 0, 1, 2$ with $i \neq j$.

The total Hamiltonian matrix $\hat{H}$ becomes a 9×9 matrix in this case. The interaction component of matrix $\hat{H}^{\text{int}}$ contains only the main diagonal

$$\hat{H}^{\text{int}} := \text{diag}(U_{00}, U_{01}, U_{02}U_{10}, U_{11}, U_{12}, U_{20}, U_{21}, U_{22}), \tag{18}$$

where U_{ij} is the energy of Coulomb interaction between i^{th} dot in line α and j^{th} dot in line β and can be calculated using formula (13). Since the interaction case with two or more electrons requires calculating the Coulomb interaction terms, one needs to consider also the distances associated with the electron locations. For this reason, the interaction case is more conveniently represented through the position representation and dot occupation numbers rather than through the energy states.

Taking the following physical parameters from [22], [35]: dot area 80 nm × 80 nm, MOS gate length 20 nm, effective mass $m^* = 1.08 \times m_0$, where $m_0 = 9.1 \times 10^{-31}$ kg is the rest mass of the electron, gate voltages set at 160 mV; and applying expressions (12), (13) and (14) on the wavefunctions obtained in the previous section, we obtain the Hamiltonian matrices for the two case studies as shown in Fig. 6. The presented matrices correspond to well-isolated dots, hence the non-diagonal elements (the tunneling terms) are quite small. By changing the gate voltages (i.e., potential energy barriers) within a range of 100 to 150 mV, one alters the non-diagonal terms that usually have an exponential sensitivity to these voltages. The energies in these Hamiltonian matrices are given in meV. We note that the Hamiltonian terms on the order of 10^{-6} and below are at the margin of the numerical accuracy of the method, and can be viewed as negligibly small.

V. CIRCUIT EQUIVALENT OF THE TIME-INDEPENDENT AND TIME-DEPENDENT SCHRÖDINGER EQUATION

By introducing a proper scale factor χ, and defining $\tilde{H}(t) = \frac{\chi}{\hbar}\hat{H}(t)$ we can write

$$\begin{cases} \chi \frac{dC_R(t)}{dt} = \tilde{H}_I(t)C_R(\tau) + \tilde{H}_R(t)C_I(\tau) \\ \chi \frac{dC_I(t)}{dt} = \tilde{H}_I(t)C_I(\tau) - \tilde{H}_R(t)C_R(\tau), \end{cases} \tag{19}$$

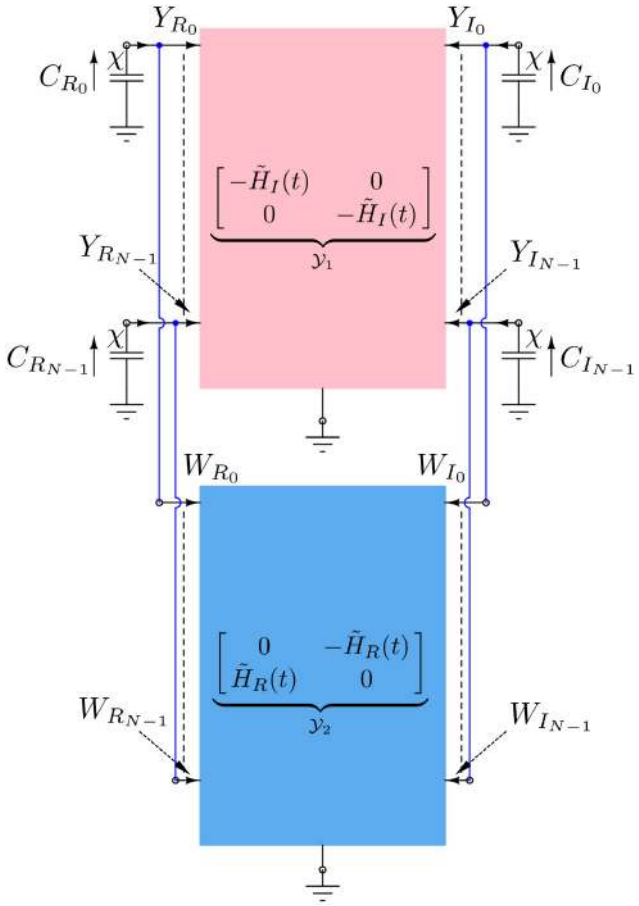

FIGURE 7. Equivalent circuit implementing (8). The real part, $C_{R_k}(t)$, and imaginary part, $C_{I_k}(t)$, of the $C_k(t)$ complex probability amplitudes of the states $|k\rangle$ are interpreted as voltages across a pair of capacitors. The $\mathcal{Y}_1$ time-varying conductance matrix implements a multi-gyrator, whereas $\mathcal{Y}_2$ represents a non-energetic multi-terminal resistor.

where $\tilde{H}_R(t) = \Re\{\tilde{H}(t)\}$, $\tilde{H}_I(t) = \Im\{\tilde{H}(t)\}$, $C_R = \Re\{C\}$, and $C_I = \Im\{C\}$. If we define

$$\begin{bmatrix} Y_R \\ Y_I \end{bmatrix} = \underbrace{\begin{bmatrix} -\tilde{H}_I(t) & 0 \\ 0 & -\tilde{H}_I(t) \end{bmatrix}}_{\mathcal{Y}_1(t)} \begin{bmatrix} C_R \\ C_I \end{bmatrix}, \tag{20}$$

and

$$\begin{bmatrix} W_R \\ W_I \end{bmatrix} = \underbrace{\begin{bmatrix} 0 & -\tilde{H}_R(t) \\ \tilde{H}_R(t) & 0 \end{bmatrix}}_{\mathcal{Y}_2(t)} \begin{bmatrix} C_R \\ C_I \end{bmatrix}, \tag{21}$$

we can interpret (19) as a set of $2N$ Kirchhoff current law equations governing the circuit in Fig. 7.

By doing so, C_R and C_I are viewed as the voltages across two sets of $2N$ identical capacitors of capacitance χ. Since $\tilde{H} = \tilde{H}^\dagger$, we have $\tilde{H}_R = \tilde{H}_R^T$, and $\tilde{H}_I$ is skewed-symmetric, i.e., $\tilde{H}_{I_{jj}} = 0$ and $\tilde{H}_{I_{jk}} = -\tilde{H}_{I_{kj}} = 0$ (for $j \neq k$). These properties reflect on $\mathcal{Y}_1$ and $\mathcal{Y}_2$ making the former a multi-gyrator [48], and the latter a non-energetic multi-terminal resistor. The energy stored in the capacitors is thus preserved, i.e., $\frac{1}{2}\chi \sum_k [C_{R_k}^2(t) + C_{I_k}^2(t)]$ holds a constant value. It is thus possible to derive the probability of a particle to be found in the state $|k\rangle$ through the energy stored in the k-th pair of capacitors. In particular, $|C_k(t)|^2 = C_{R_k}^2(t) + C_{I_k}^2(t)$, for $k = 0, \ldots, N-1$, corresponds to the probability of a particle to be found in state $|k\rangle$.

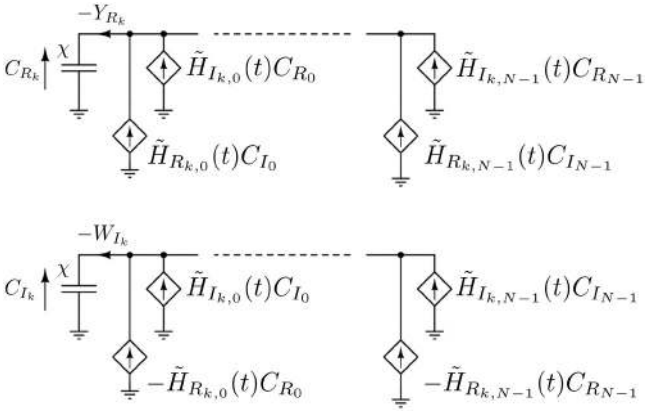

FIGURE 8. Schematic referring to the k-th pair of capacitors in Fig. 7 and thus involving the k-th row of both $\tilde{H}_R$ and $\tilde{H}_I$.

The internal structure of the multi-terminal elements in Fig. 7 can be achieved by resorting to time-varying[1] voltage-controlled current sources as sketched in Fig. 8. Since typically $\tilde{H}(t)$ is sparse, only a limited amount of controlled sources is needed. Obviously, in case $\tilde{H}(t)$ is real, the multi-gyrator vanishes and so do the corresponding sources in Fig. 8.

We remark that the synthesis of the multi-terminal components in Fig. 7 is not aimed at deriving a low-level description of these electrical devices. This means that it is not relevant to achieve a typical electrical device that realizes each controlled current source shown in Fig. 8. Actually, we are just interested in a high-level synthesis that allows to easily implement the dynamics inherent to (19) in a circuit simulator.

VI. NUMERICAL EXAMPLES

The simulations described in this section were performed by resorting to the circuit simulator PAN [49], [50].

The simulation duration for the two examples described in this section, limited by the numerical solution of the state equations, was almost 60 s on a laptop equipped with Intel(R) Core(TM) i7-5600U CPU @ 2.60GHz and 16.0 GB RAM. On average, the number of states introduced by qubits that we can simulate within a reasonable CPU time with conventional numerical approaches is 10^5. We implement partitioning techniques that split the equivalent model into a non-linear sub-part and in a linear one. In some peculiar cases, the number of states can be increased to 10^6 and above. We remark that the circuit simulator PAN is still not

1. Depending on the adopted circuit simulator, these time-varying components can be implemented by resorting to different strategies. In our simulator PAN [49], [50], for instance, one can choose either the Spice like formalism or the Verilog-A one.

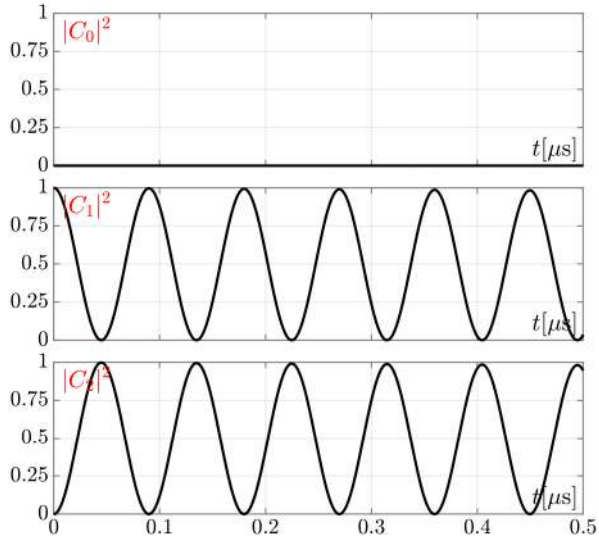

FIGURE 9. The case study of one electron in three dots: probability to occupy the three dots as a function of time (time axis is in [μs]).

optimized for these kind of simulations, and consequently, there is room for future development.

A. A VERY SIMPLE CASE

The first example refers to a 3-dot 1-line system. In this case, the structure of the Hamiltonian matrix is reported in (16) in the position representation, and the numerical values of its entries are shown in Fig. 6(a). As was mentioned earlier, this reference case corresponds to well-isolated dots. The elements of the matrix imply that tunneling (transitions) are possible (although with the small probabilities) between the states $|1\rangle$ and $|2\rangle$ while the rate of tunneling between the states $|0\rangle$ and $|1\rangle$ and $|0\rangle$ and $|2\rangle$ is negligibly small or zero.

Concerning the equivalent circuit used to emulate (19), we choose $\chi = \frac{\hbar}{10^{-3}e}$ F (where e is the magnitude of electron charge) to observe the dynamic evolution of the system on a proper time-scale in s, and use the entries of the Hamiltonian matrix without converting them into J. The initial conditions were chosen as $C_R(0) = [0, 1, 0]^{\mathrm{T}}$ and $C_I(0) = [0, 0, 0]^{\mathrm{T}}$. The selection of the initial conditions is not very important, but in our case it means that the electron starts in one of the edge dots labeled in the position basis as $|1\rangle$.

When presenting the results of numerical simulations, we can visualize the probability of states. Figure 9 shows the time evolution of the states (in the position representation). One of the states is zero (up to the accuracy of numerical integration) and the other two states display occupation oscillations which correspond to the tunneling of the electron from one edge dot to another edge dot. At the same time, one can note that $|C_0|^2 + |C_1|^2 + |C_2|^2 = 1$ and the normalization condition is preserved.

This case illustrates an interesting example of oscillations that occur between the two edge dots, skipping completely the middle dot. While it may seem unusual, such oscillations can be easily understood from the energy spectrum shown in Fig. 5. Due to a specific symmetry of the system, the states that correspond to the location of an electron in the edge left or right dot form a split energy level. Because there is no overlap in the wavefunctions $|0\rangle$ and $|1\rangle$ and the wavefunctions $|0\rangle$ and $|2\rangle$, and the system is considered to be isolated (no mechanism to pump or remove energy), the equilibrium oscillations occur only between the two levels with the same energy, which happen to correspond to the edge dots. This effect can also be confirmed with a topological theory.

B. A MORE COMPLEX CASE STUDY

This second example refers to a 3-dot $\times$ 2-line system and we use the position representation. In this case, the structure of the overall Hamiltonian matrix is captured by (17) and reported in Fig. 6(b) (the units of the matrix entries are meV). The results are presented in Fig. 10.

Concerning the equivalent circuit used to emulate (19), we choose once more $\chi = \frac{\hbar}{10^{-3}e}$ F. The initial conditions were fixed at $C_R(0) = [0, 0, 0, 0, 1, 0, 0, 0, 0]^{\mathrm{T}}$ and $C_I(0) = [0, 0, 0, 0, 0, 0, 0, 0, 0]^{\mathrm{T}}$ for the simulations shown in Figs. 10(a)–(b), and $C_R(0) = [0, 0, 0, 0, 0, 1, 0, 0, 0]^{\mathrm{T}}$ and $C_I(0) = [0, 0, 0, 0, 0, 0, 0, 0, 0]^{\mathrm{T}}$ for the simulations shown in Fig. 10(c). The agreement on the initial conditions can be understood from Fig. 6(b) where the state $|11\rangle$, which corresponds to the initial occupation on the edge left dot in line α and also the edge left dot in line β, is described by the fifth component of the state vector. All other states do not contribute to the initial conditions.

When presenting the results, we must understand now that each probability amplitude derived from the entries of the equivalent circuit state vector corresponds to a state of the combined system. For example, the first entry in the state vector $|C_0(t)|^2 = C_{R_0}^2(t) + C_{I_0}^2(t)$ corresponds to the probability of the electron in line α to occupy dot 0 while, at the same time, the electron in line β also occupies its respective dot 0. As follows from the tensor product, there are nine combined states possible.

The six states of interest in our case are the probability p_0^α to locate the electron in dot zero of line α regardless of the state of the electron in line β; the probability p_1^α to locate the electron in dot 1 of line α regardless of the state of the electron in line β; the probability p_2^α to locate the electron in dot 2 of line α regardless of the state of the electron in line β; and the three counterpart probabilities $p_{0,1,2}^\beta$ for the electron in line β. These are expressed as follows:

$$\begin{aligned} p_0^\alpha &= |C_0(t)|^2 + |C_1(t)|^2 + |C_2(t)|^2 \\ p_1^\alpha &= |C_3(t)|^2 + |C_4(t)|^2 + |C_5(t)|^2 \\ p_2^\alpha &= |C_6(t)|^2 + |C_7(t)|^2 + |C_8(t)|^2 \\ p_0^\beta &= |C_0(t)|^2 + |C_3(t)|^2 + |C_6(t)|^2 \\ p_1^\beta &= |C_1(t)|^2 + |C_4(t)|^2 + |C_7(t)|^2 \\ p_2^\beta &= |C_2(t)|^2 + |C_5(t)|^2 + |C_8(t)|^2 \end{aligned} \tag{22}$$

The case study of two interacting particles in accordance with the interaction and tunneling terms in the Hamiltonian

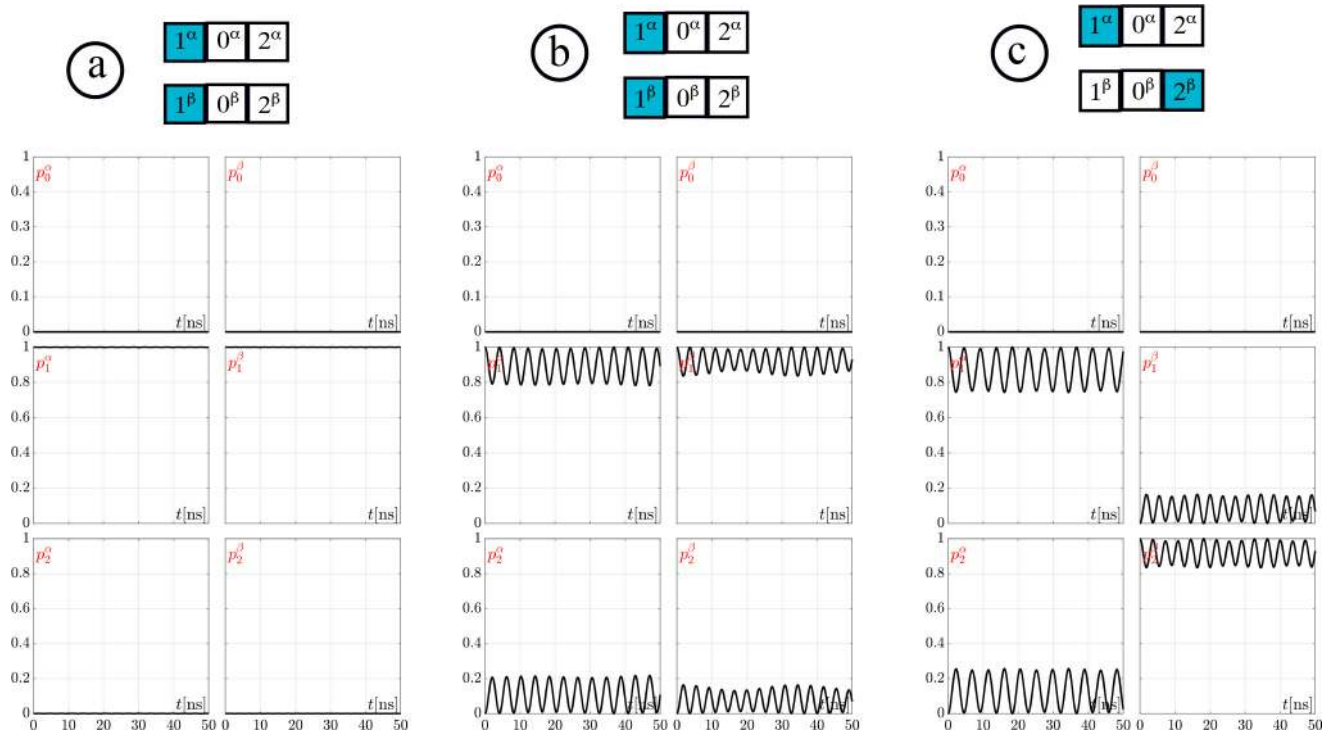

FIGURE 10. Case study of two interacting particles in two lines α and β showing the dot occupation probability with time. The effect of the interaction and tunneling terms in the Hamiltonian matrix and the initial conditions is presented in this figure. The initial conditions are schematically shown on top by highlighting the initially occupied dot by blue. (a) The case of the reference Hamiltonian from Fig. 6(b) shows no change in the dot occupation probability with time since the interaction between the particles is too strong. (b) The case when the diagonal elements of the Hamiltonian matrix are reduced by 30% and the tunneling terms are increased 10 times shows synchronous oscillations of charges. (c) The case when the diagonal elements of the Hamiltonian matrix are reduced by 30% and the tunneling terms are increased 10 times shows oscillations of charges in the opposite dots.

matrix and the initial conditions is presented in Fig. 10 in the form of the dot occupation probabilities as a function of time. The initial conditions are schematically shown at the top of the figure by highlighting the initially occupied dot with the blue color. Figure 10(a) shows the case of the reference Hamiltonian matrix from Fig. 6(b) that, as mentioned earlier, corresponds to well-isolated dots and strong electrostatic interaction (since the straightforward formula of the Coulomb Law (14) with no screening effect was used to calculate the matrix). The initial conditions correspond to the left edge dot in line α and left edge dot in line β being occupied at the initial instance of time. There is no change of the dot occupation probabilities over time in this case since electrons are strongly repelled (with no possibility to increase their separation) and there is not enough tunneling energy to allow them to tunnel through.

In order to observe some dynamics, we have increased the tunneling terms tenfold (they are controlled by the imposer voltages and feature an exponential sensitivity) and decreased the interaction terms by 30%. Having the same initial conditions as in the simulation from subfigure (a), one observes synchronous oscillations of dot occupation probabilities in subfigure (b), implying that electrons are coupled and move synchronously between the edge dots. Similar effects of synchronized motion in QD arrays have been reported in [51]. Finally, the case shown in subfigure (c) illustrates a different type of initial conditions when electrons start in the opposite dots in lines α and β and oscillate in 'anti-phase' due to the electrostatic repelling force between them.

VII. DISCUSSION ON INCORPORATING DEPHASING PHENOMENA AND TEMPERATURE DEPENDENCE

So far we have considered an isolated quantum system, without any external fluctuations that may appear due to interactions with the system's environment. Such effects arise mainly from the coupling between the quantum system under consideration and the environment, a phenomenon which is usually denoted as quantum decoherence. In particular, charge noise is the main effect of dephasing (decoherence) in quantum systems that are based on the manipulation of single electrons. This will lead eventually to the loss of fidelity. In this section, we would like to examine how temperature effects and decoherence can be taken into account.

The discussed model can be easily extended to include dephasing phenomena by the use of the theory of open quantum systems [52]–[54]. However, the description of the system will have to be done through a *density matrix* rather than a state vector. In the ideal case, we have assumed that our system is described by an ensemble of pure states, i.e., the system can be described by a ket $|\psi\rangle$. However, in the most general case, one deals with mixed states. For example,

when one wishes to include an ensemble at thermal equilibrium or to formulate independently the prepared states, then a statistical treatment is a necessity in order to describe quantum observables. In such a case, it is useful to introduce the density matrix.

To take into account the temperature effects, a mixed state density matrix is used, which is defined as follows:

$$\rho = \sum_k p_k |\psi_k\rangle\langle\psi_k|. \tag{23}$$

Here, p_k gives the classic probabilities to occupy given states $|\psi\rangle_k$. These probabilities appear in the matrix following the principles of Statistical Mechanics. If we assume that the system has a contact with a thermal bath, each quantum state can be occupied only with some probability. These probabilities are related to the absolute temperature T (in kelvin units) and the energies E_k of the states as $p_k \propto \exp(-\beta E_k)$ where $\beta = 1/(k_B T)$, k_B is Boltzmann's constant. The above matrix is known as the thermal density matrix.

The density matrix is also subject to a differential equation. While the state vector is governed by the Schrödinger equation (6), the density matrix is governed by the Liouville–von Neumann equation that is derived from the Schrödinger equation:

$$\dot{\rho} = -\frac{i}{\hbar}[H, \rho]. \tag{24}$$

Here, the pair of brackets denotes a commutator of two operators (in our case $[H, \rho] = H\rho - \rho H \neq 0$). For example, in the three-dot study case, the wavefunction is represented as $|\phi\rangle = (c_0, c_1, c_2)$ with c_k $(k = 0, 1, 2)$ being the probability amplitudes of the basis states $|0\rangle$, $|1\rangle$ and $|2\rangle$. The pure state (no temperature effects) density matrix in this case becomes:

$$\rho = |\psi\rangle\langle\psi| = \begin{pmatrix} |c_0|^2 & c_0\, c_1^* & c_0\, c_2^* \\ c_0^*\, c_1 & |c_1|^2 & c_1\, c_2^* \\ c_0^*\, c_2 & c_1^*\, c_2 & |c_2|^2 \end{pmatrix}, \tag{25}$$

which is a Hermitian matrix. One can see, similarly to the state vector, that the density matrix also contains the information about the probability amplitudes c_k, but in a different form. Furthermore, the Lindblad equation of the density matrix can be used if one wants to model the decoherence effects. With regard to the methodology of equivalent circuits presented in this paper, the decomposition described in Section V should be applied to eq. (24) rather than to eq. (6) if the temperature effects and decoherence are to be taken into account.

VIII. DISCUSSION ON CO-SIMULATION OF QUANTUM DOT ARRAY REGISTER AND CONTROL ELECTRONICS

The model described by eq. (19) can be implemented in a testbench that integrates the quantum dot array shown in Fig. 2 with control and detection electronics [22], [35]. The preferred language for this modeling is Verilog-AMS, which can be compiled and executed by a time-domain simulator such as Cadence Spectre. With this approach, the analog interface circuits can be coupled to the quantum dot array seamlessly while the Verilog-AMS platform offers a diverse range of mathematical functions to model the states of interest in the quantum register. The testbench environment can be enhanced to model the impairments in the quantum register and electronic circuitry. The model inputs are the simulation timestamps and the real-time imposer voltages. The process starts as the imposer voltage is elevated by the control circuitry. At each subsequent timestamp, the probability of the states of interest are calculated. Those states are associated with nodes coupled to the detector circuitry. The process stops with the lowering of imposer voltage and the computed probabilities are frozen; and from those probabilities a bi-modal distribution is generated. One sample from that distribution is selected and scaled to an analog voltage to be used as register output. This output is processed by the detector chain and can be sampled by the testbench over many iterations for statistical analysis.

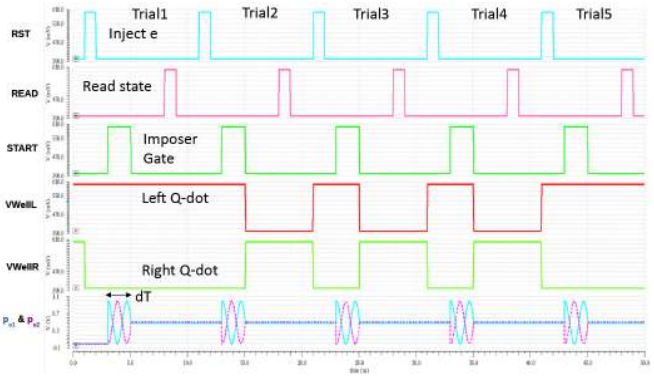

FIGURE 11. Time-domain signal waveforms from and into the quantum dot array [55]. This snapshot shows the first five trials of the quantum experiment with dT of 2 ns. The probabilities of states are shown in the last row in the chart.

An example of a time-domain Spectre co-simulation of the quantum dot array with its control electronics is shown in Fig. 11 [55]. The quantum structure used in this simulation is a simple two-dot system separated by a single imposer. Each quantum dot is connected to a "quantum point contact" (QPC) and their respective voltages are V_{WellL} and V_{WellR}. The QPCs are directly coupled to the detector circuits. The model is written in Verilog-A and the inputs to it are the RST, START, and READ signals that are asserted by an on-chip controller. The RST signal initializes the QPCs to a predefined DC voltage. The START signal controls the imposer gate with a pulse width dT. The READ signal commands the detector to take a snapshot of the QPC voltage. The model continuously computes the probabilities of the states of the two quantum dots from the rising edge of START, as shown in the bottom trace of Fig. 11. The process stops at the falling edge of START and. At that point, V_{WellL} and V_{WellR} voltages are generated by randomly selecting a sample from the bi-modal distribution as mentioned earlier. Those voltages are sampled by the detector at the rising edge of READ signal and are stored in the database. The sequence of RST, START, and READ signals are repeated every 10 ns

over a period of 10 us and all the recorded samples analyzed during post processing. All critical parameters, such as DC biases, detector high and low voltages, and dT, can be swept to perform a regression analysis.

IX. DISCUSSION AND CONCLUSION

This paper presented a methodology to describe quantum mechanical states of charge qubits (electrons placed in coupled quantum dots) using equivalent electrical circuits. The choice of the studied system was motivated by recent advances in semiconductor (particularly CMOS) qubit technologies. We have provided a detailed description of the system and the general mathematical formalism of quantum wave mechanics. We showed how to relate the equations to simulations of wave functions and we explained the relationship between the parameters appearing in the resulting model and the parameters of the physical system under study. An efficient methodology to obtain 2D wave functions was outlined. Using this methodology, simulations corresponding to the quantum dot arrays fabricated in a CMOS technology and recently published in the literature are presented. The generalization of quantum mechanical equations, their conversion to equivalent circuits, and two numerical examples are discussed. The two examples are illustrative but simple enough, with the second example illustrating two interacting electrons.

Some specific highlights of this study include:

- Solving a problem in the context of time-independent wave mechanics requires one to obtain time independent functions ϕ_n that provide the information about the probability density of particle(s) in a given potential energy, calculating the matrix elements H_{mn} (7) and solving the set of ordinary differential equations (6).
- For this reason, once the functions ϕ_n are obtained, formulating the ODEs is straightforward. In general, a set of ODEs can be conveniently presented as an electrical network or solved using a package suitable for circuit modeling.
- The reason we believe the electrical network representation may be convenient is that there are a number of packages optimized to work with circuit design and simulations, as well as a number of analysis tools (e.g., working with noise) designed specifically for circuits.
- In addition to the point above, the probability amplitudes in this representation can be related to the variables of an equivalent electrical circuit. This interpretation of probabilities may be used for the analysis and modeling of interface circuitry. Since this particular study is aimed at CMOS qubits, we briefly discussed how to incorporate charge readout. Other types of readout (e.g., dispersive) may also be incorporated into this methodology.
- Temperature and decoherence effects can be incorporated if the description in terms of the density matrix, rather than the state vector, is used. In this case, an electrical network representation should be attempted on the Liouville–von Neumann equation (that is derived from the Schrödinger equation).
- In order to estimate the parameters of the equivalent circuit, time-independent wave functions are most important. While solving the full time-dependent Schrödinger equation is challenging, solving a time-independent equation on single-electron wave functions can be made effective. In this study, we tried a technique developed for sparse matrices, and it returned a very good result.
- Once the ODEs representing the dynamics of the wave function are formulated and presented in the form of an equivalent electrical network, there is no reason the result obtained from simulating the electrical network should be different than that obtained from the wave equation.
- Two case studies were presented and discussed. The simpler case study included one line of three dots that can accommodate one electron. This case study was used to test the methodology. However, even in this simple case, oscillations between the edge dots are possible due to the specific symmetry of the system.
- The second case study included two lines, each containing three dots and each accommodating one electron (two electrons in total). Hence, this example included interaction between the electrons. Depending on initial conditions, either synchronous motion of the charges or ‘anti-phase’ oscillations can be seen. Similar effects were reported earlier, hence indirectly confirming the validity of the results.

REFERENCES

[1] P. Benioff, “The computer as a physical system: A microscopic quantum mechanical hamiltonian model of computers as represented by Turing machines,” *J. Stat. Phys.*, vol. 22, no. 5, pp. 563–591, 1980.

[2] R. P. Feynman, “Simulating physics with computers,” *Int. J. Theor. Phys.*, vol. 21, nos. 6–7, pp. 467–488, 1982.

[3] P. W. Shor, “Algorithms for quantum computation: Discrete logarithms and factoring,” in *Proc. 35th Annu. Symp. Found. Comput. Sci.*, Santa Fe, NM, USA, 1994, pp. 124–134.

[4] J. Preskill, “Quantum computing in the NISQ era and beyond,” *Quantum*, vol. 2, p. 79, Aug. 2018.

[5] *IBM Quantum Experience*. Accessed: Aug. 22, 2021. [Online]. Available: https://quantum-computing.ibm.com

[6] Y. Wang, Y. Li, Z.-Q. Yin, and B. Zeng, “16-qubit IBM universal quantum computer can be fully entangled,” *NPJ Quantum Inf.*, vol. 4, no. 1, pp. 1–6, 2018.

[7] M. Kjaergaard *et al.*, “Superconducting qubits: Current state of play,” *Annu. Rev. Condens. Matter Phys.*, vol. 11, pp. 369–395, Mar. 2020.

[8] F. Arute *et al.*, “Quantum supremacy using a programmable superconducting processor,” *Nature*, vol. 574, no. 7779, pp. 505–510, 2019.

[9] P. Kok, W. J. Munro, K. Nemoto, T. C. Ralph, J. P. Dowling, and G. J. Milburn, “Linear optical quantum computing with photonic qubits,” *Rev. Mod. Phys.*, vol. 79, no. 1, p. 135, 2007.

[10] J. L. O’brien, A. Furusawa, and J. Vučković, “Photonic quantum technologies,” *Nat. Photon.*, vol. 3, no. 12, pp. 687–695, 2009.

[11] C. D. Bruzewicz, J. Chiaverini, R. McConnell, and J. M. Sage, “Trapped-ion quantum computing: Progress and challenges,” *Appl. Phys. Rev.*, vol. 6, no. 2, 2019, Art. no. 021314.

[12] N. W. Hendrickx *et al.*, “A four-qubit germanium quantum processor,” *Nature*, vol. 591, no. 7851, pp. 580–585, 2021.

[13] M. Brooks, “Beyond quantum supremacy: The hunt for useful quantum computers,” *Nature*, vol. 574, no. 7776, pp. 19–22, 2019.

[14] Y. A. Pashkin, T. Yamamoto, O. Astafiev, Y. Nakamura, D. V. Averin, and J. S. Tsai, “Quantum oscillations in two coupled charge qubits,” *Nature*, vol. 421, no. 6925, pp. 823–826, 2003.

[15] L. C. L. Hollenberg *et al.*, "Charge-based quantum computing using single donors in semiconductors," *Phys. Rev. B, Condens. Matter*, vol. 69, no. 11, 2004, Art. no. 113301.
[16] K. D. Petersson, J. R. Petta, H. Lu, and A. C. Gossard, "Quantum coherence in a one-electron semiconductor charge qubit," *Phys. Rev. Lett.*, vol. 105, no. 24, 2010, Art. no. 246804.
[17] T. Fujisawa, G. Shinkai, T. Hayashi, and T. Ota, "Multiple two-qubit operations for a coupled semiconductor charge qubit," *Physica E, Low Dimensional Syst. Nanostruct.*, vol. 43, no. 3, pp. 730–734, 2011.
[18] Y.-C. Yang, S. Coppersmith, and M. Friesen, "Achieving high-fidelity single-qubit gates in a strongly driven charge qubit with 1/f charge noise," *NPJ Quantum Inf.*, vol. 5, no. 1, p. 12, 2019.
[19] B. Lucatto, D. S. Koda, F. Bechstedt, M. Marques, and L. K. Teles, "Charge qubit in van der waals heterostructures," *Phys. Rev. B, Condens. Matter*, vol. 100, Sep. 2019, Art. no. 121406(R).
[20] G. X. Chan and X. Wang, "Suppression of leakage for a charge qubit in triangular triple quantum dots," *Adv. Quantum Technol.*, vol. 2, no. 12, 2019, Art. no. 1900072.
[21] F. Ansaloni *et al.*, "Single-electron operations in a foundry-fabricated array of quantum dots," *Nat. Commun.*, vol. 11, no. 1, pp. 1–7, 2020.
[22] I. Bashir *et al.*, "A single-electron injection device for CMOS charge qubits implemented in 22-nm FD-SOI," *IEEE Solid-State Circuits Lett.*, vol. 3, pp. 206–209, 2020.
[23] S. J. Pauka *et al.*, "A cryogenic CMOS chip for generating control signals for multiple qubits," *Nat. Electron.*, vol. 4, no. 1, pp. 64–70, 2021.
[24] R. B. Staszewski, I. Bashir, E. Blokhina, and D. Leipold, "Cryo-CMOS for quantum system on-chip integration: Quantum computing as the development driver," *IEEE Solid-State Circuits Mag.*, vol. 13, no. 2, pp. 46–53, Jun. 2021.
[25] L. Zong *et al.*, "Nanopurification of silicon from 8% to 99.99% purity with a simple and scalable process," *Proc. Nat. Acad. Sci.*, vol. 112, no. 44, pp. 13473–13477, 2015.
[26] E. Charbon *et al.*, "15.5 Cryo-CMOS circuits and systems for scalable quantum computing," in *Proc. IEEE Int. Solid-State Circuits Conf. (ISSCC)*, San Francisco, CA, USA, 2017, pp. 264–265.
[27] B. Patra, *et al.*, "Cryo-CMOS circuits and systems for quantum computing applications," *IEEE J. Solid-State Circuits*, vol. 53, no. 1, pp. 309–321, Jan. 2018.
[28] I. Bashir *et al.*, "A mixed-signal control core for a fully integrated semiconductor quantum computer system-on-chip," in *Proc. IEEE Eur. Solid-State Circuits Conf. (ESSCIRC)*, Cracow, Poland, 2019, pp. 1–4.
[29] H. Bluhm and L. R. Schreiber, "Semiconductor spin qubits–A scalable platform for quantum computing?" in *Proc. IEEE Int. Symp. Circuits Syst. (ISCAS)*, Sapporo, Japan, 2019, pp. 1–5.
[30] S. R. Ekanayake, T. Lehmann, A. S. Dzurak, R. G. Clark, and A. Brawley, "Characterization of SOS-CMOS FETs at low temperatures for the design of integrated circuits for quantum bit control and readout," *IEEE Trans. Electron Devices*, vol. 57, no. 2, pp. 539–547, Feb. 2010.
[31] N. Lee *et al.*, "Enhancing electrostatic coupling in silicon quantum dot array by dual gate oxide thickness for large-scale integration," *Appl. Phys. Lett.*, vol. 116, no. 16, 2020, Art. no. 162106.
[32] R. Li *et al.*, "A crossbar network for silicon quantum dot qubits," *Sci. Adv.*, vol. 4, no. 7, 2018, Art. no. eaar3960.
[33] C. H. Yang *et al.*, "Operation of a silicon quantum processor unit cell above one kelvin," *Nature*, vol. 580, no. 7803, pp. 350–354, 2020.
[34] F. A. Zwanenburg *et al.*, "Silicon quantum electronics," *Rev. Mod. Phys.*, vol. 85, no. 3, p. 961, 2013.
[35] A. Esmailiyan *et al.*, "A fully integrated DAC for CMOS position-based charge qubits with single-electron detector loopback testing," *IEEE Solid-State Circuits Lett.*, vol. 3, pp. 354–357, 2020.
[36] G. Kron, "Electric circuit models of the schrödinger equation," *Phys. Rev.*, vol. 67, nos. 1–2, p. 39, 1945.
[37] E. Blokhina, P. Giounanlis, A. Mitchell, D. R. Leipold, and R. B. Staszewski, "CMOS position-based charge qubits: Theoretical analysis of control and entanglement," *IEEE Access*, vol. 8, pp. 4182–4197, 2019.
[38] W. I. L. Lawrie *et al.*, "Quantum dot arrays in silicon and germanium," *Appl. Phys. Lett.*, vol. 116, no. 8, 2020, Art. no. 080501.
[39] C. K. Maiti, *Introducing Technology Computer-Aided Design (TCAD): Fundamentals, Simulations, and Applications*. Singapore: Taylor & Francis Group and Pan Stanford, 2017.
[40] S. A. Vitale, P. W. Wyatt, N. Checka, J. Kedzierski, and C. L. Keast, "FDSOI process technology for subthreshold-operation ultralow-power electronics," *Proc. IEEE*, vol. 98, no. 2, pp. 333–342, Feb. 2010.
[41] J. Tiffenberg *et al.*, "Single-electron and single-photon sensitivity with a silicon skipper CCD," *Phys. Rev. Lett.*, vol. 119, no. 13, 2017, Art. no. 131802.
[42] R. Zhao *et al.*, "Single-spin qubits in isotopically enriched silicon at low magnetic field," *Nat. Commun.*, vol. 10, no. 1, pp. 1–9, 2019.
[43] R. Maurand *et al.*, "A CMOS silicon spin qubit," *Nat. Commun.*, vol. 7, no. 1, pp. 1–6, 2016.
[44] D. J. Griffiths and D. F. Schroeter, *Introduction to Quantum Mechanics*. Cambridge, U.K.: Cambridge Univ. Press, 2018.
[45] R. Shankar, *Principles of Quantum Mechanics*. New York, NY, USA: Springer, 2012.
[46] J. J. Sakurai and E. D. Commins, *Modern Quantum Mechanics, Revised Edition*. Boston, MA, USA: Addison-Wesley, 1994.
[47] H. De Raedt and K. Michielsen, "Algorithm to solve the time-dependent schrödinger equation for a charged particle in an inhomogeneous magnetic field: Application to the Aharonov–Bohm effect," *Comput. Phys.*, vol. 8, no. 5, pp. 600–607, 1994.
[48] A. G. J. Holt and R. L. Linggard, "Multiterminal gyrator," *Proc. Inst. Elect. Eng.*, vol. 117, no. 8, pp. 1591–1598, 1970.
[49] F. Bizzarri, A. Brambilla, G. S. Gajani, and S. Banerjee, "Simulation of real world circuits: Extending conventional analysis methods to circuits described by heterogeneous languages," *IEEE Circuits Syst. Mag.*, vol. 14, no. 4, pp. 51–70, 4th Quart., 2014.
[50] F. Bizzarri and A. Brambilla, "PAN and MPanSuite: Simulation vehicles towards the analysis and design of heterogeneous mixed electrical systems," in *Proc. New Gener. CAS (NGCAS)*, Genova, Italy, 2017, pp. 1–4.
[51] B. Szafran, "Paired electron motion in interacting chains of quantum dots," *Phys. Rev. B, Condens. Matter*, vol. 101, no. 7, 2020, Art. no. 075306.
[52] G. Schaller, *Open Quantum Systems Far From Equilibrium*, vol. 881. Cham, Switzerland: Springer, 2014.
[53] F. Tabakin, "Model dynamics for quantum computing," *Ann. Phys.*, vol. 383, pp. 33–78, Aug. 2017.
[54] P. Giounanlis *et al.*, "CMOS charge qubits and qudits: Entanglement entropy and mutual information as an optimization method to construct CNOT and SWAP gates," *Semicond. Sci. Technol.*, vol. 36, no. 9, 2021, Art. no. 095014.
[55] I. Bashir, P. Giounanlis, E. Blokhina, D. Leipold, K. Pomorski, and R. B. Staszewski, "A Verilog-A model of the shuttle of an electron in a two quantum-dot system," in *Proc. 17th IEEE Int. New Circuits Syst. Conf. (NEWCAS)*, Munich, Germany, Jun. 2019, pp. 1–4.

ELENA BLOKHINA (Senior Member, IEEE) received the M.Sc. degree in physics and the Ph.D. degree in physical and mathematical sciences from Saratov State University, Russia, in 2002 and 2006, respectively, and the Habilitation HDR degree in electronic engineering from UPMC Sorbonne Universities, France, in 2017.

From 2005 to 2007, she was a Research Scientist with Saratov State University. Since 2019, she has been with Equal1 Labs, where she is currently a CTO. Her research interests include the analysis, design, modeling and simulations of nonlinear circuits, systems and networks with particular application to complex, mixed-domain, and multiphysics systems.

Dr. Blokhina is a the Chair Elect of the IEEE Technical Committee on Nonlinear Circuits and Systems. She had been elected to serve as a member of the Boards of Governors of the IEEE Circuits and Systems Society form 2013 to 2015, and she has been re-elected from 2015 to 2017. She has served as the Programme Co-Chair of the first edition of IEEE Next Generation of Circuits and Systems Conference 2017, and the IEEE International Conference on Electronics, Circuits and Systems. From 2016 to 2017, she was an Associate Editor for IEEE TRANSACTIONS ON CIRCUITS AND SYSTEMS—I: REGULAR PAPERS, and since 2018 she has been the Deputy Editor in Chief of IEEE TRANSACTIONS ON CIRCUITS AND SYSTEMS—I: REGULAR PAPERS. She has served as a member of organizing committees, review and programme committees, a session chair, and a track chair at many leading international conferences on circuits, systems and electronics, including the IEEE International Symposium on Circuits and Systems.

ANDRII SOKOLOV received the B.Sc. degree in computational physics and M.Sc. degree in theoretical physics from Odessa National I. I. Mechnikov University, Ukraine, in 2009 and 2010 respectively. He is currently pursuing the Ph.D. degree with the School of Electrical and Electronic Engineering, University College and is a part time Researcher with Equal1 Labs. His research is funded by CONNECT, the Science Foundation Ireland Research Centre for Future Networks and Communications. He has coauthored publications on simulation of electromagnetic and electrostatic microelectromecahnical systems and quantum systems coupled with control circuit interfaces. His research interests include modeling and simulation methods of multiphysics and nonlinear systems, high-performance computation, and time series analysis. He serves as a reviewer for conferences and journals curated by IEEE Circuits and Systems Society.

PANAGIOTIS GIOUNANLIS received the B.Sc. degree in physics and the M.Sc. degree in computational physics from the Aristotle University of Thessaloniki, Greece, in 2008 and 2011, respectively, and the Ph.D. degree in 2017, for his research on the modeling of nonlinear effects for micro-scale devices and their application to reliability and control by the use of both numerical and analytical approaches. He has been a Postdoctoral Senior Physicist with Equal 1 Labs since September 2017. He is contributing to the work strand on simulation and design of CMOS qubits, quantum gates, and quantum neural networks, providing theoretical and modeling support for quantum system-on-chip (QSOC) design. He is also a member of a team of researchers in developing analytical and computational methods for the characterization and simulation of physical models of silicon quantum dots and quantum experiments. He is also working in multiparticle modeling of interaction and entanglement of spin, hybrid and charge based qubits, the modeling of decoherence and noise effects, the description of quantum transport, and interaction of silicon qubits by the theory of open quantum systems. His research interests include: modeling and simulation of microscale devices and complex systems, solid-state physics, and computational quantum mechanics.

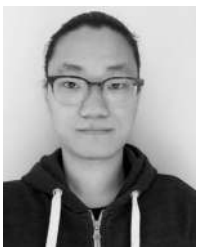

XUTONG WU received the B.E. degree in electronic and information engineering from the University of Electronic Science and Technology of China in 2018, and the M.E. degree in computer and electronic engineering from University College Dublin in 2020. He is currently pursuing the Ph.D. degree with the School of Electrical and Electronic Engineering, University College Dublin, and is a Software Engineer with Equal1 Labs. His research interests are in modeling and simulation of CMOS qubits, quantum algorithms, and quantum computing.

IMRAN BASHIR (Member, IEEE) received the B.S.E.E. degree *(summa cum laude)* from the University of Texas at Arlington in 2001, and the M.S.E.E. and Ph.D. degrees from the University of Texas at Dallas in 2008 and 2014. He joined Texas Instruments in 2002, and he was elected the prestigious title of Group Member of Technical Staff in 2006. He played a key role in the productization of GSM/EDGE SoCs based on the Digital RF Processor technology. In 2009, he joined NVidia Inc., and worked on 2G/3G/4G multimode cellular radios. In 2014, he worked as a Mixed-Signal IC Designer with a start-up called Senseeker Engineering Inc., where he designed read-out circuits for IR image sensors. During the Fall of 2015, he was a Senior Research Fellow of the School of Electrical and Electronic Engineering, University College Dublin, Dublin, Ireland. He was with Cypress Semiconductor Corp. from 2015 and 2018. In 2019, he joined Equal1 Labs, where he currently is a Fellow. In addition to his day-time job, he has volunteered as an Officer for the SSCS and CASS local chapters. He is also a member of Tau Beta Pi.

DIRK LEIPOLD (Senior Member, IEEE) received the Diploma degree in physics from the University of Konstanz in 1991, and the Ph.D. degree in physics in 1995. Since 1995, he has been working in semiconductor physics, semiconductor circuits and semiconductor circuit system design at various semiconductor OEM and start-up companies and he has created over 150 patents on semiconductor device design, cell phone circuitry, and optical sensor design. He has created innovative circuit concepts, such as the Digital Radio Processor at Texas Instruments, allowing the integration of cell phone radio front-end in a digital CMOS process and the first high volume CMOS power amplifier for cell phones. These products have been deployed in over two billion devices worldwide. Since 2015, he has been working on a foundry SOI quantum computer based on entangled quantum aperture logic (equal) which allows very dense quantum computer implantation as single chip. He is currently a CEO of Equal1, where he has been working on a commercial quantum computer solution based on the CMOS technology.

ROBERT BOGDAN STASZEWSKI (Fellow, IEEE) was born in Bialystok, Poland. He received the B.Sc. *(summa cum laude)*, M.Sc., and Ph.D. degrees in electrical engineering from the University of Texas at Dallas, Richardson, TX, USA, in 1991, 1992, and 2002, respectively. From 1991 to 1995, he was with Alcatel Network Systems, Richardson, TX, USA, involved in SONET cross-connect systems for fiber optics communications. He joined Texas Instruments Incorporated, Dallas, TX, USA, in 1995, where he was an elected Distinguished Member of Technical Staff (limited to 2% of technical staff). From 1995 to 1999, he was engaged in advanced CMOS read channel development for hard disk drives. In 1999, he co-started the Digital RF Processor (DRP) Group within Texas Instruments with a mission to invent new digitally intensive approaches to traditional RF functions for integrated radios in deeply-scaled CMOS technology. He was appointed as a CTO of the DRP Group from 2007 to 2009. In 2009, he joined the Delft University of Technology, Delft, The Netherlands, where currently he holds a guest appointment of a Full Professor (*Antoni van Leeuwenhoek Hoogleraar*). Since 2014, he has been a Full Professor with the University College Dublin, Dublin, Ireland. He is also a Co-Founder of a startup company, Equal1 Labs, with design centers located in Silicon Valley and Dublin, Ireland, aiming to produce single-chip CMOS quantum computers. He has authored or coauthored five books, seven book chapters, 140 journal and 210 conference publications, and holds 210 issued U.S. patents. His research interests include nanoscale CMOS architectures and circuits for frequency synthesizers, transmitters and receivers, as well as quantum computers. He was a TPC Chair of 2019 ESSCIRC in Krakow, Poland. He was a recipient of the 2012 IEEE Circuits and Systems Industrial Pioneer Award. In May 2019, he received the title of Professor from the President of the Republic of Poland. He recently jointed the TPC of VLSI Symposium on Circuits.

ANGELO BRAMBILLA (Member, IEEE) received the Dr.Ing. degree in electronics engineering from the University of Pavia, Pavia, Italy, in 1986. He is a Full Professor with the Dipartimento di Elettronica, Informazione e Bioingegneria, Politecnico di Milano, Milano, Italy, where he has been working in the areas of circuit analysis, simulation, and modeling.

FEDERICO BIZZARRI (Senior Member, IEEE) was born in Genoa, Italy, in 1974. He received the Laurea (M.Sc.) five-year degree (*summa cum laude*) in electronic engineering and the Ph.D. degree in electrical engineering from the University of Genoa, Genoa, Italy, in 1998 and 2001, respectively. Since October 2018, he has been an Associate Professor with the Electronic and Information Department, Politecnico di Milano, Milan, Italy. He is a Research Fellow of the Advanced Research Center on Electronic Systems for Information and Communication Technologies "E. De Castro," University of Bologna, Italy. He served as an Associate Editor of the IEEE TRANSACTIONS ON CIRCUITS AND SYSTEMS—PART I from 2012 to 2015, and he was awarded as one of the 2012–2013 Best Associate Editors of IEEE TRANSACTIONS ON CIRCUITS AND SYSTEMS—PART I.